Mesoscale plastic texture in body-centered cubic metals under uniaxial load

R. Gröger,[1,*] V. Vitek,[2] and T. Lookman[3]

[1]*Central European Institute of Technology & Institute of Physics of Materials (CEITEC IPM), Academy of Sciences of the Czech Republic, Žižkova 22, Brno 61600, Czech Republic*

[2]*University of Pennsylvania, Department of Materials Science and Engineering, 3231 Walnut Street, Philadelphia, Pennsylvania 19104, USA*

[3]*Los Alamos National Laboratory, Theoretical Division, MS B262, Los Alamos, New Mexico 87545, USA*

(Received 13 July 2017; published 8 November 2017; publisher error corrected 26 February 2018)

We develop a minimal continuum dislocation dynamics model for slip in bcc metals that accounts explicitly for non-Schmid behavior of screw dislocations in these materials. The dislocation substructure is represented by a continuum distribution of 1/2[111] screw dislocations moving on three possible {110} planes according to the flow rule that describes the response of isolated screw dislocations to external loads. The cross-slip of dislocations is assessed using the master equation which takes into account different energy barriers for dislocations moving on the three slip planes. To demonstrate the performance of the model, we study the buildup of plastic strain at 77 K in both tension and compression for a number of loading directions covering the entire area of the standard stereographic triangle. The non-Schmid behavior of screw dislocations is shown to persist to the continuum level, whereby interactions between dislocations merely affect the rate of plastic flow.

DOI: 10.1103/PhysRevMaterials.1.063601

I. INTRODUCTION

Plastic deformation of crystalline solids is a complex process that takes place on a wide range of length scales and involves a variety of dislocation mechanisms. At the length scale comparable with interatomic distances and the time scale short compared with the mean inverse frequency of dislocation reactions, the plastic deformation may be viewed as the motion of individual dislocations driven by the external load. This is often considered to be uniform in the region inside which the dislocation glide is investigated. Such studies have been made using pair potentials [1], empirical central-force many body potentials [2,3], and potentials that explicitly take into account the quantum mechanical aspects of bonding and thus include the directionality of atomic bonds [4–6]. The latter are indispensable in understanding the fundamental mechanisms responsible for different behavior of dislocations in non-close-packed structures in contrast with close-packed metals [7].

Understanding the evolution of dislocation substructure at the microscale and the macroscopic behavior of materials requires a physically based coarse-graining methodology that is both based on correct physics and is computationally efficient. This may be accomplished by treating each characteristic scale with a different model and requiring that the predictions of these different models match at the boundaries of their validity. This approach allows one to treat each length scale with the right physics by employing methods based on first principles [8], atomistic models [3], discrete dislocation dynamics [9], and crystal plasticity finite element methods [10]. The main challenge of this methodology is to combine these conceptually different methods into one unified framework, where the results of the lower-level simulation represent input into the higher-level model [11,12]. A conceptually different but theoretically not less demanding approach is to develop a field-theoretical model rooted at the mesoscale that is purported to describe some range of length and time scales of interest [13]. This requires that the formulation of the model captures as closely as possible the essential physics responsible for the microstructure evolution on these scales.

Due to the inherent difficulty in treating many scales by a single model, most approximate descriptions of plasticity developed so far assume isotropic elasticity to describe long-range interactions between dislocations [14,15]. Moreover, they take the plastic flow of close-packed metals as a paradigm and tacitly assume the validity of the Schmid law that is inherent in von Mises and Tresca yield criteria. This approach is fully justified in the metals with close-packed structures (fcc and hcp) since in this case the only stress component involved in the planar dislocation glide is the shear stress in the slip direction (Burgers vector) in the slip plane and the Schmid law applies. However, this is not the case in a large class of crystalline materials with more open crystal structures [16], in particular body-centered cubic (bcc) metals in which the Schmid law is well known to break down [7]. The reason is that in these metals the plastic deformation is controlled by the motion of screw dislocations, which is opposed by a large lattice friction arising from their nonplanar cores [7,16–19]. This nonplanarity of dislocation cores leads to an intrinsic asymmetry of the Peierls barrier and this asymmetry is even further enhanced during core transformations induced by applied stresses. The motion of screw dislocations is thus a thermally activated process [20,21] during which the dislocation core is transformed so as to overcome local Peierls barriers, which generally depend on the full applied stress tensor. Hence the activation enthalpy for this process is a nontrivial function of the applied stress tensor.

In principle, it could be determined using molecular dynamics. An alternative is to employ an approximate physically justified model of thermally activated dislocation glide. Such model has been proposed, for example, by Dorn and Rajnak [22] and recently advanced to take into account the full applied stress tensor [23]. It was proposed recently that the Peierls barrier and its stress dependence can be determined using the nudged elastic band (NEB) method [24]. The ensuing model

*groger@ipm.cz

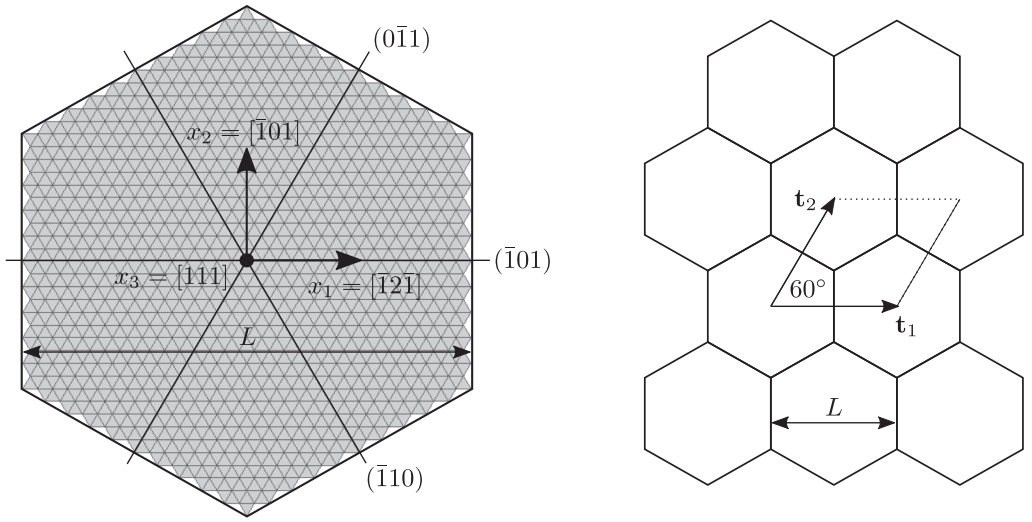

FIG. 1. Computational cell and its periodic tiling: (a) discretization of the simulation cell by equilateral triangular elements; (b) periodic tiling of the simulation grid in (a) using two primitive translation vectors $\boldsymbol{t}_1$ and $\boldsymbol{t}_2$. All 1/2[111] screw dislocations and their Burgers vectors are perpendicular to the plane of the figure.

of the dislocation motion then determines the stress at which the glide of a single screw dislocation is initiated [23,24].

In recent years, there has been an increased interest in formulating continuum models of plastic deformation for bcc metals using the yield criteria that capture the breakdown of the Schmid law in these materials [25,26] and a similar development has been taking place in the discrete dislocation dynamics [27,28]. In this paper we employ the above-mentioned model of the thermally activated dislocation motion [23] in developing a mesoscopic description of the plastic flow that incorporates all non-Schmid effects found in previous molecular statics simulations of isolated screw dislocations at 0 K [29]. Specifically, these include the well-known twinning-antitwinning asymmetry of the flow stress that is controlled by the shear stresses in the directions of the Burgers vectors applied in the planes of dislocation glide, as well as shear stresses perpendicular to the Burgers vectors [19,29]. Besides respecting elastic anisotropy of bcc metals when evaluating the long-range elastic fields of dislocations, this model contains also the effects of temperature and plastic strain rate.

II. THEORETICAL BACKGROUND

Molecular statics simulations [19,29] provide ample evidence that isolated $1/2\langle 111\rangle$ screw dislocations move under stress at 0 K by elementary steps on three {110} planes in the zone of the $\langle 111\rangle$ axis. We have asserted before [29] that the macroscopically observed slip on other planes such as {211} or {321} can be explained by composite slip of the dislocation on two adjacent {110} planes. In the following, we thus consider the simplest nontrivial computational cell shown in Fig. 1(a), whereby 1/2[111] screw dislocations may move between the nearest lattice sites on three different {110} planes, in particular $(\bar{1}01)$, $(0\bar{1}1)$, and $(\bar{1}10)$. Both positive and negative orientations of these dislocations are taken into account, which results in six relevant slip systems in our model. These are $(\bar{1}01)[111]$, $(0\bar{1}1)[111]$, $(\bar{1}10)[111]$ and their conjugates $(\bar{1}01)[\bar{1}\bar{1}\bar{1}]$, $(0\bar{1}1)[\bar{1}\bar{1}\bar{1}]$, $(\bar{1}10)[\bar{1}\bar{1}\bar{1}]$. Hereafter, the first three slip systems will be referred to by the superscript $s+$ and the latter three by the superscript $s-$.

The simulation cell in Fig. 1(a) will be discretized with equilateral triangles. This is necessary to avoid numerical artifacts when differentiating the dislocation density along nonorthogonal slip planes, as argued already in Ref. [30]. The dislocation density will be represented by the scalar field $\rho(\boldsymbol{x}) = N_d(\boldsymbol{x})/S_\perp$, where N_d is the number density of dislocations at the position $\boldsymbol{x}$ piercing the area $S_\perp$, which will be taken as the area of each triangular cell in Fig. 1(a). In the calculations, the dislocation density will be resolved at the corners of the grid as ρ^n, where $n = 1, \ldots, n_{\text{node}}$, where n_{node} is the number of nodes of the grid. For the purpose of visualization, ρ^n will be interpolated into the interior of each triangular cell using the three-node bilinear shape functions. The simulation cell is assumed to be periodic along the trace of each {110} plane, as shown in Fig. 1(b). This is accomplished using two translation vectors $\boldsymbol{t}_1 = L(1,0)$ and $\boldsymbol{t}_2 = L(0.5, \sqrt{3}/2)$, where L is the width of the block along any of the three {110} planes.

The stress field due to an arbitrary dislocation density is calculated using Stroh's sextic theory [31], explained in the book of Hirth and Lothe [32]. If the stress field corresponding to N_d^n dislocations at the node n, whose position is $\boldsymbol{x}_d^n$, in an *infinite* simulation cell is $\boldsymbol{\sigma}^\infty(\boldsymbol{x}; \boldsymbol{x}_d^n)$, the total stress field due to a triangular array of these dislocations with nearest neighbor separation equal to L is

$$\boldsymbol{\sigma}(\boldsymbol{x}; \boldsymbol{x}_d^n) = \sum_{i_2=-\infty}^{\infty} \sum_{i_1=-\infty}^{\infty} \boldsymbol{\sigma}^\infty\big(\boldsymbol{x}; \boldsymbol{x}_d^n + i_1\boldsymbol{t}_1 + i_2\boldsymbol{t}_2\big). \quad (1)$$

The total stress field due to dislocations assigned to all n_{node} nodes is then obtained as

$$\boldsymbol{\sigma}(\boldsymbol{x}) = \sum_{n=1}^{n_{\text{node}}} \boldsymbol{\sigma}\big(\boldsymbol{x}; \boldsymbol{x}_d^n\big). \quad (2)$$

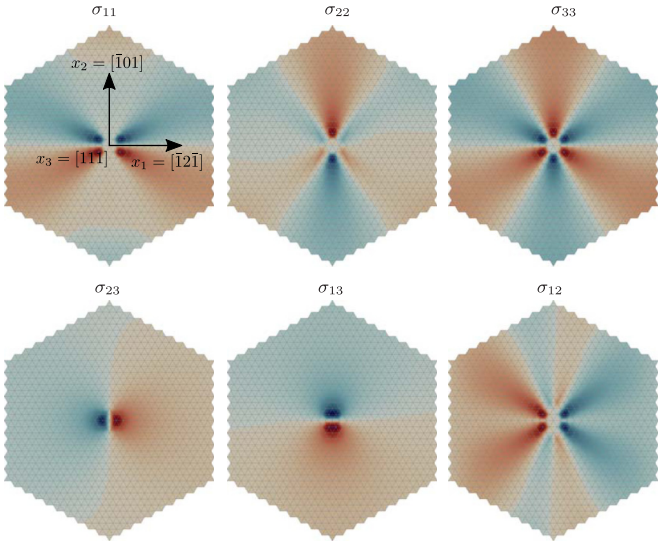

FIG. 2. Stress field around the $1/2[111]$ screw dislocation at the origin due to a superposition of the like dislocations generated by periodic boundary conditions. The color map ranges from dark blue (largest negative value) via gray (zero) to dark red (largest positive value). It is symmetric in all figures but differs for each component in order to visualize its spatial variation. These fields were calculated using the elastic constants for bcc Mo.

For practical purposes, it is sufficient to consider only the terms in (1) that correspond to a few smallest absolute values of i_1 and i_2. Here, we have considered i_1 and i_2 to range from -1 to 1 and verified that the results of the simulation did not change significantly when more images were taken into account.

For illustration, the stress field around a $1/2[111]$ screw dislocation in a periodic triangular array of the like dislocations is shown in Fig. 2. All components of the stress field are nonzero which is unlike the well-known elastic solution for isotropic materials, where only the σ_{13} and σ_{23} components are nonzero [32]. This complexity arises due to a combination of the elastic anisotropy of the material and the special orientation of the simulation block, where the three axes are not parallel to $\langle 100\rangle$ directions.

We implicitly assume the existence of dislocation sources and annihilations between dislocations in that the two processes result in a steady-state evolution of the dislocation density ρ. Hence the evolution law for the dislocation density takes the form of the continuity equation

$$\dot{\rho}^{s\pm} + \left(\rho^{s\pm} v_l^{s\pm}\right)_{,l} = 0, \tag{3}$$

where comma means differentiation with respect to individual coordinate axes. Because the motion of $1/2\langle 111\rangle$ screw dislocations in bcc metals is thermally activated, their velocities are [21,33]

$$v^{s\pm} = \pm v_0 \exp\left(-\frac{H^s_{\rm act}}{kT}\right), \tag{4}$$

where v_0 is related to the frequency of dislocation oscillations in the ground state and $H^s_{\rm act}$ is the activation enthalpy to move the dislocation on the slip system s. The velocity $v^{s\pm}$ is assigned the direction that moves the dislocations in positive/negative direction on the slip plane corresponding to the system s.

We have shown in previous studies that the Peierls stress of a single dislocation is a nontrivial function of the shear stresses parallel and perpendicular to the slip direction, which are referred to in the following as nonglide stresses. These data gave rise to the stress dependence of the activation enthalpy that was investigated in [24,34] for a large number of combinations of the shear stresses parallel and perpendicular to the slip directions and orientations of the plane in which the shear stress parallel to the slip direction is the largest, the so-called maximum resolved shear stress plane (MRSSP). It has been shown in [34] that the activation enthalpy can be closely approximated as

$$H^s_{\rm act} = A\left\{B - \tanh\left[C\left(\log\frac{\tau^{*s}}{\tau^*_{cr}} + D\right)\right]\right\}, \tag{5}$$

where τ^{*s} is an effective stress that involves a particular combination of stresses exerted on the slip system s and includes all effects of nonglide stresses. The critical value of the effective stress is the yield stress τ^*_{cr} for which the dislocation will move at 0 K. The coefficients A, B, C, D are obtained by the following reasoning. If the applied stress on some slip system s is zero, i.e., also $\tau^{*s} = 0$, $H_{\rm act}$ reaches its maximum which is the energy of two isolated kinks, $2E_k$. This is typically obtained from experiments at the temperature for which the dislocation glide ceases to be thermally activated, i.e., the temperature dependence of the flow stress reaches a plateau. The other extreme is when τ^{*s} reaches τ^*_{cr} for which the dislocation is moved purely mechanically without the need for any thermal activation and thus $H^s_{\rm act} = 0$. Due to these constraints, only two coefficients in (5) are independent and were determined in [34] by fitting the dependence of $H^s_{\rm act}$ on τ^{*s}/τ^*_{cr} for the most highly stressed slip system s, i.e., $(\bar{1}01)[111]$, using the models developed in Refs. [22,23].

A particularly simple form of the effective stress τ^{*s} in (5), proposed by Qin and Bassani [35], involves a linear combination of four stresses, two of which are parallel and two perpendicular to the slip direction,

$$\tau^{*s} = \tau^s_0 + a_1\tau^s_1 + a_2\tau^s_2 + a_3\tau^s_3, \tag{6}$$

where $\tau^s_0 = \hat{\boldsymbol{m}}^s \boldsymbol{\Sigma} \hat{\boldsymbol{n}}^s$ is the shear stress parallel to the slip direction (unit vector $\hat{\boldsymbol{m}}^s$) and acts in the slip plane with unit normal $\hat{\boldsymbol{n}}^s$. The total stress $\boldsymbol{\Sigma}$ is obtained as a sum of the externally applied load $\boldsymbol{\sigma}^{\rm ext}$ and the internal stress $\boldsymbol{\sigma}^{\rm int}$ due to the superposition of the stress fields of all dislocations and their images. The second term of (6) is $\tau^s_1 = \hat{\boldsymbol{m}}^s \boldsymbol{\Sigma} \hat{\boldsymbol{n}}^s_1$ and, together with the first term, captures the twinning-antitwinning asymmetry observed in all bcc metals. The last two terms, $\tau^s_2 = (\hat{\boldsymbol{n}}^s \times \hat{\boldsymbol{m}}^s)\boldsymbol{\Sigma}\hat{\boldsymbol{n}}^s$ and $\tau^s_3 = (\hat{\boldsymbol{n}}^s_1 \times \hat{\boldsymbol{m}}^s)\boldsymbol{\Sigma}\hat{\boldsymbol{n}}^s_1$, capture the influence of shear stresses perpendicular to the slip direction on the activation of individual slip systems. So far, the coefficients a_1, a_2, a_3 and the yield stress τ^*_{cr} have been estimated only for bcc Mo and W [36]; the parametrizations for Ta, Nb, V, Cr, and α-Fe are underway.

The conserved continuum dislocation dynamics (3) must be complemented by a model of thermally activated cross-slip of dislocations. The probability with which the dislocation density ρ^s appears in the total dislocation density is $P^s = \rho^s / \sum_{s'} \rho^{s'}$, where $\sum_s P^s = 1$. The associated master

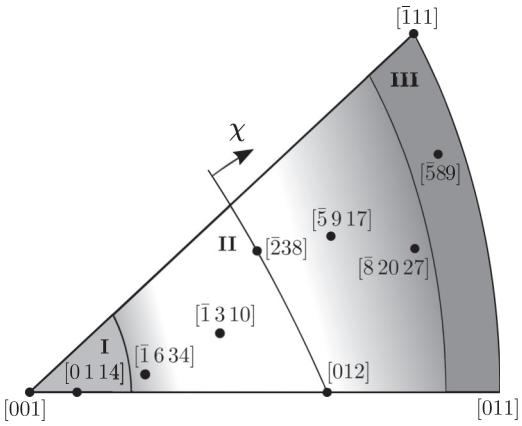

FIG. 3. Orientations of the applied load considered for mesoscopic simulations carried out in this paper. The standard stereographic triangle is divided into three regions marked I, II, III each of which corresponds to a different slip activity and thus the plastic texture. Here, χ is the angle between the $(\bar{1}01)$ plane and the MRSSP corresponding to a particular loading axis.

equation [37] is then

$$\frac{dP^s}{dt} = \sum_{s'(\neq s)} (\nu^{s'\to s} P^{s'} - \nu^{s\to s'} P^s), \tag{7}$$

where the first term corresponds to dislocations cross-slipping to s from other systems s' and the second term to dislocations cross-slipping from s to other systems s'. The rate of cross-slip of the dislocation from the slip system s to another system s' is defined as $\nu^{s\to s'} = \nu_0 \exp(-H^{s'}_{\text{act}}/kT)$.

The new dislocation density in the slip system s after the thermally activated cross-slip event is then $\rho^s(t+\Delta t) = P^s(t+\Delta t)\sum_{s'} \rho^{s'}(t)$, which reassigns dislocations to individual slip systems while preserving the total number of dislocations. Without the assumption of steady state with respect to the generation and recombination of dislocations, this equation should be complemented also by the rates of dislocation generation and annihilation [38].

III. MESOSCOPIC TEXTURE UNDER UNIAXIAL LOAD

In the following simulations, we demonstrate the performance of the model by investigating the evolution of mesoscopic texture for loading in tension and compression along the axes shown in Fig. 3 and comparing it to existing experimental observations of slip traces. We consider bcc Mo for which the following parameters were used: atomic-level lattice parameter, $a_0 = 3.1472$ Å [6]; mesoscopic lattice parameter, $a = 100a_0 \approx 31.4$ nm; temperature, $T = 77$ K; elastic constants, $C_{11} = 464.7$ GPa, $C_{12} = 161.5$ GPa, and $C_{44} = 108.9$ GPa [6]; parameters of the yield criterion, $a_1 = 0.24$, $a_2 = 0$, $a_3 = 0.35$, and $\tau^*_{cr} = 1014$ MPa [36]; parameters of the activation enthalpy, $A = 0.90$, $B = 0.41$, $C = 0.60$, and $D = 0.73$ [34]; velocity of free dislocations, $v_0 = 1$ cm/s [39,40]; maximum cross-slip frequency is chosen as $\nu_0 = 10^2$ s^{-1}. The hexagonal simulation cell was discretized by 7080 triangular elements with 30 elements along the trace of each {110} plane. This yields the width of the simulation cell, and thus periodicity along the three planes, of approximately 1 μm.

The elementary shear strain generated by a moving group of dislocations in the slip system s during the time step Δt can be obtained as a scalar field $\Delta\gamma^{s\pm} = \rho^{s\pm} b v^{s\pm} \Delta t$, which is a time-discretized version of the Orowan equation [32]. The plastic strain due to all positive and negative dislocations in the six slip systems is then $\Delta\gamma = \sum_s (\Delta\gamma^{s+} + \Delta\gamma^{s-})$. The cummulative plastic strain at each point of the grid generated by dislocations in all slip systems between the time $t = 0$ and any further time T is then $\gamma = \sum_{t=0}^{T} \Delta\gamma(t)$.

The evolution of the density of positive and negative dislocations in the three slip systems ($\rho^{s\pm}$) has been calculated by the method developed in the preceding section and terminated when the total dislocation density assigned to the three slip systems no longer changes. The steady-state scalar fields $\gamma(\boldsymbol{x})$ obtained for three characteristic orientations in the regions I, II, III in Fig. 3 are shown in Fig. 4.

The calculated plastic texture $\gamma(\boldsymbol{x})$ for loading directions in the region II of the stereographic triangle is shown in Fig. 4(b) for tension and in Fig. 4(e) for compression. In both cases, the plastic deformation occurs predominantly due to dislocations moving on $(\bar{1}01)$ planes, which is the most highly stressed {110} plane of the [111] zone. For loading directions in the region III of the stereographic triangle, shown in Fig. 4(c) for tension and in Fig. 4(f) for compression, most of the slip activity arises due to screw dislocations moving on $(\bar{1}10)$ planes, which is manifested by strong texture along the trace of this plane. For loading in compression, the plastic deformation occurs also on the $(\bar{1}01)$ plane, but this represents only a minor contribution to the overall plastic strain. Figures 4(a) and 4(d) show the plastic texture for loading in tension and compression in the region I of the stereographic triangle. In both cases, most of the slip activity takes place on the $(\bar{1}01)$ plane. The loading in compression also activates secondary slip on the $(0\bar{1}1)$ plane, which is often associated with anomalous slip [41]. Depending on the precise orientation of the loading axis, this amounts to at most 30% of the total plastic strain.

For comparison, we plot in Fig. 5 the histogram that shows for each loading axis the amount of slip contributed by dislocations moving on the three {110} planes under tension and compression. The $(\bar{1}01)$ slip controls the plastic flow for loading in the center-triangle orientations up to roughly halfway towards $\chi = \pm 30^\circ$. For loading axes in the region of large positive χ, the plastic flow is predominantly due to dislocations moving on $(\bar{1}10)$ planes, with minor contribution of the $(\bar{1}01)$ slip. This non-Schmid behavior is more significant in tension than in compression. On the other hand, loading in compression corresponding to $\chi \to -30^\circ$ generates anomalous slip on the $(0\bar{1}1)$ plane. The prominence of this anomalous slip reaches about 30% for the loading axis corresponding to the most negative value of χ considered here. It should be emphasized that the observation of slip on $(0\bar{1}1)$ and $(\bar{1}10)$ planes is due primarily to the third and fourth terms in (6) and their effects on the parameters A, B, C, and D in (5).

The results for tension compare well with the experiments on high-purity Mo single crystals by Kitajima *et al.* [42] made at 4.2 K and those carried by Aono *et al.* [43] at 77 K, both of which reveal slip traces on the $(\bar{1}01)$ plane for most orientations in the stereographic triangle. For loading

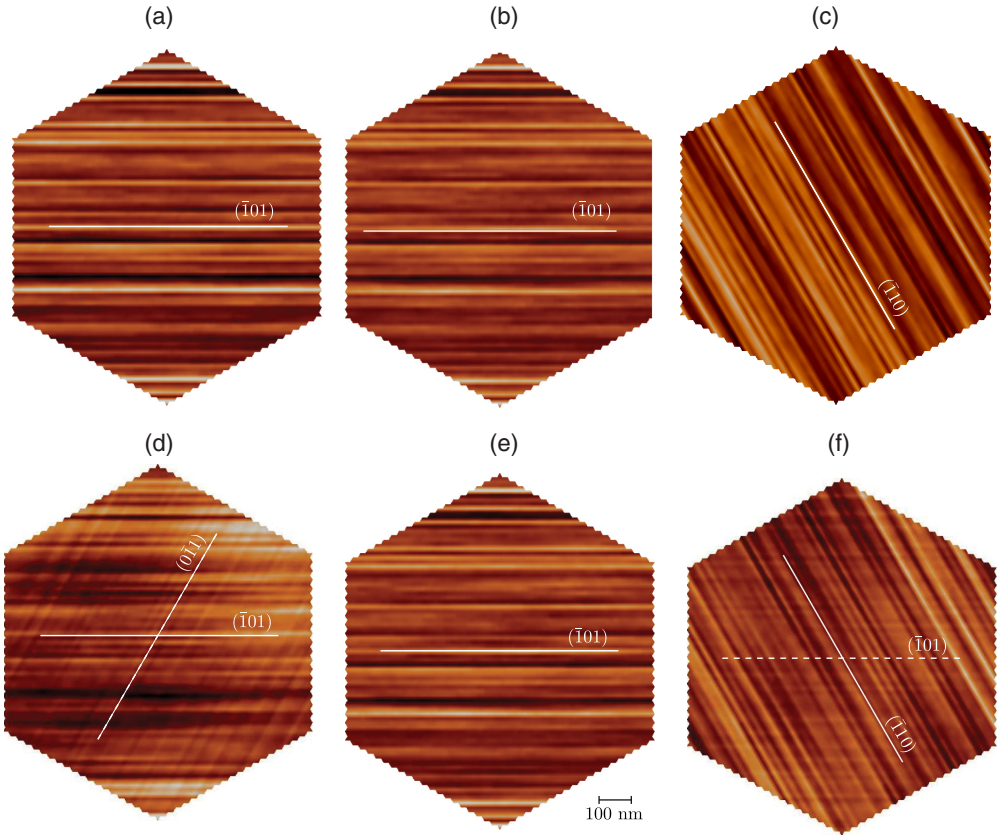

FIG. 4. Steady-state plastic texture represented by the cummulative plastic strain $\gamma(\boldsymbol{x})$ obtained for uniaxial loading at 77 K along the axes shown in Fig. 3: (a) tension [0 1 14], (b) tension [$\bar{2}38$], (c) tension [$\bar{5}89$], (d) compression [0 1 14], (e) compression [$\bar{2}38$], and (f) compression [$\bar{5}89$]. The primary slip plane that carries most of the plastic strain is marked by solid line and the secondary slip plane by dashed line. The scale bar is the same in all figures. The color scale corresponds to the values of γ between -1.5×10^{-3} (black) and 1.5×10^{-3} (white).

directions close to its $[011] - [\bar{1}11]$ edge, these experiments show slip predominantly on the $(\bar{1}10)$ plane. For very low temperatures (cf. 4.2 K experiments [42]), the change of the slip plane occurs abruptly as the loading direction reaches the $[011] - [\bar{1}11]$ edge of the triangle. This transition becomes more gradual at 77 K [43], where the transition from the $(\bar{1}01)$ slip to the $(\bar{1}10)$ slip takes place for $\chi = 5$–15° for tension and $\chi = 15 - 20^\circ$ for compression. Our results obtained for

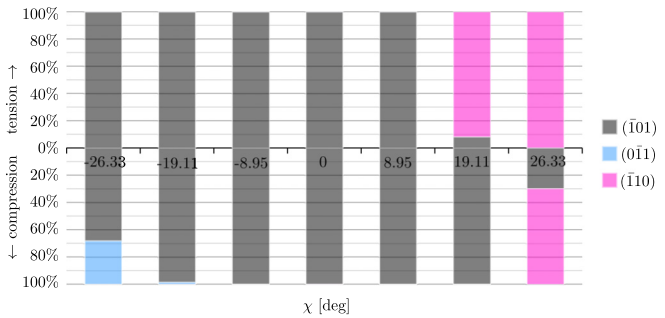

FIG. 5. Histogram showing the fractions of the total plastic strain contributed by slip on the three {110} planes for loading in tension (upper part) and compression (lower part) along the axes in Fig. 3. The blue and purple bars correspond to the mesoscopic plastic texture that cannot be reconciled with the Schmid law.

compression agree well with the experiments of Jeffcoat *et al.* on pure Mo [44] and on dilute Mo-Nb and Mo-Re alloys [45], where compression along the direction in the central part of the stereographic triangle resulted in dominant slip on the $(\bar{1}01)$ plane. The partial change of the slip plane for $\chi > 10^\circ$ from $(\bar{1}01)$ to $(\bar{1}10)$ predicted in the previous section agrees with the slip trace analyses in Refs. [44,45], where compression in the directions closer to the $[011] - [\bar{1}11]$ edge of the stereographic triangle resulted in "irrational slip" on two different high-index planes, one close to $(\bar{1}01)$ and the other close to $(\bar{1}10)$. Our observations made for compression at $\chi \ll 0^\circ$ are in qualitative agreement with the slip trace analyses in Refs. [44,45]. The predicted minor role of the $(0\bar{1}1)$ anomalous slip in Mo under compression close to the [001] corner of the stereographic triangle agrees with the experiments of Marichal *et al.* on W [46,47], where it amounts only to 9% of the total plastic strain.

The most important aspect of the computer simulations made in this paper is that the non-Schmid behavior of isolated dislocations persists to higher temperatures. This enters the model through the parametrization of the activation enthalpy (5) and the effective yield criterion (6), both of which in general differ from material to material as shown by comparing Mo and W in Refs. [23,29,36]. The glide of dislocations in VIB group metals (Cr, Mo, W) on $(0\bar{1}1)$ planes represents only a minor contribution to the overall plastic strain [45–47]. On the

contrary, in VB metals (V, Nb, Ta), the anomalous $(0\bar{1}1)$ slip is a dominant mode of plastic deformation at low temperatures [48–50]. The parametrization of the effective yield criteria and activation enthalpies for these materials is currently underway and will be used in the future to demonstrate the universality of the model developed here.

IV. CONCLUSIONS

We have developed a minimal version of a continuum dislocation dynamics for glide of $1/2[111]$ screw dislocations on three different planes of the [111] zone. The dislocation content is described as densities of positive and negative dislocations in each system that evolve in response to the stress fields exerted on each dislocation by the applied stress, other dislocations, and their periodic images. The velocities of dislocations are determined from the activation enthalpy that has been determined with the help of molecular statics simulations of $1/2[111]$ screw dislocations under the uniform applied stress. The probability of the cross-slip of screw dislocations into other slip planes has been evaluated using the master equation, where the rate of cross-slip depends on the activation enthalpy to move the dislocation on the cross-slip plane.

This model has been used to study the evolution of plastic strain generated by the collective motion of a large number of positive and negative $1/2[111]$ screw dislocations on their three {110} slip planes. These simulations have been made for tension and compression at 77 K for a number of loading axes covering the entire area of the standard stereographic triangle. Although the glide of dislocations is driven by the shear stress parallel to the slip direction acting in the slip plane (the Schmid stress), it is also significantly affected by the shear stresses parallel to the slip direction acting in different {110} planes and the shear stresses perpendicular to the slip direction. In all cases, interactions between dislocations only renormalize the critical stress at which dislocations move (and thus the time scale on which the dislocation density evolves) but do not modify the non-Schmid behavior of individual dislocations.

For loading the Mo single crystal along the directions in the central part of the stereographic triangle, the $1/2[111]$ dislocations move on the $(\bar{1}01)$ plane, which is the plane with the highest resolved shear stress parallel to the slip direction. This agrees well with the prediction of the Schmid law. However, the slip mechanism differs significantly for directions close to the [001] corner and $[011]-[\bar{1}11]$ edge of the triangle. For directions close to the $[011]-[\bar{1}11]$ edge, most of the plastic strain is due to dislocations moving on the $(\bar{1}10)$ plane with only a minor contribution of the $(\bar{1}01)$ slip in the case of compression. On the other hand, for the directions close to the [001] corner of the triangle, most of the plastic strain is carried by dislocations moving on the $(\bar{1}01)$ plane with a minor contribution from the $(0\bar{1}1)$ slip in compression. These predictions agree well with available low-temperature experiments on high-purity Mo single crystals made under tension and compression [42–45]. The estimate of the amount of anomalous slip compares well with recent microcompression experiments [46,47].

The conceptual simplicity of the mesoscopic model developed in this paper allows for systematic incorporation of dislocation sources and recombinations of opposite dislocations. The main ingredients that distinguish this model from existing phenomenological models is that it explicitly takes into account the non-Schmid contributions to the activation enthalpy and thus to the flow stress of individual isolated $1/2[111]$ screw dislocations. The mesoscopic model formulated here will be extended in the future to shed light onto the mechanisms that cause vastly different prominence of anomalous slip on the $(0\bar{1}1)$ plane in the metals of VB and VIB group as well as to investigation of the dislocation substructure in α-Fe.

ACKNOWLEDGMENTS

Discussions with Anter El-Azab on the discretization of nonorthogonal simulation cells are highly appreciated. The authors acknowledge financial support from the Czech Science Foundation Grant No. 16-13797S (R.G.) and from the Department of Energy, BES Grant No. DEFG02-98ER45702 (V.V.). This research was carried out under the project CEITEC 2020 (LQ1601) with financial support from the Ministry of Education, Youth and Sports of the Czech Republic under the National Sustainability Programme II.

[1] V. Vitek, Proc. R. Soc. London A **352**, 109 (1976).
[2] G. J. Ackland and V. Vitek, Phys. Rev. B **41**, 10324 (1990).
[3] M. S. Duesbery and V. Vitek, Acta Mater. **46**, 1481 (1998).
[4] J. A. Moriarty, W. Xu, P. Söderlind, J. Belak, L. H. Yang, and J. Zhu, J. Eng. Mater. Technol. **121**, 120 (1999).
[5] L. H. Yang, P. Söderlind, and J. A. Moriarty, Philos. Mag. A **81**, 1355 (2001).
[6] M. Mrovec, D. Nguyen-Manh, D. G. Pettifor, and V. Vitek, Phys. Rev. B **69**, 094115 (2004).
[7] J. W. Christian, Metall. Trans. A **14**, 1237 (1983).
[8] S. L. Frederiksen and K. W. Jacobsen, Philos. Mag. **83**, 365 (2003).
[9] H. R. Piehler, ASM Handbook **22A**, 232 (2009).
[10] I. J. Beyerlein and A. Hunter, Philos. Trans. R. Soc. London A **374**, 20150166 (2016).
[11] N. M. Ghoniem, E. P. Busso, N. Kioussis, and H. Huang, Philos. Mag. **83**, 3475 (2003).
[12] F. Roters, P. Eisenlohr, L. Hantcherli, D. D. Tjahjanto, T. R. Bieler, and D. Raabe, Acta Mater. **58**, 1152 (2010).
[13] N. Goldenfeld, B. P. Athreya, and J. A. Dantzig, J. Stat. Phys. **125**, 1019 (2006).
[14] M. Koslowski, A. M. Cuitiño, and M. Ortiz, J. Mech. Phys. Solids **50**, 2597 (2002).
[15] S. Sreekala and M. Haataja, Phys. Rev. B **76**, 094109 (2007).
[16] V. Vitek and V. Paidar, in *Dislocations in Solids*, edited by J. P. Hirth (Elsevier, Amsterdam, 2008), Vol. 14, pp. 439–514.
[17] M. S. Duesbery, in *Dislocations in Solids*, edited by F. R. N. Nabarro (Elsevier, Amsterdam, 1989), Vol. **8**, pp. 66–173.
[18] V. Vitek, Prog. Mater. Sci. **36**, 1 (1992).
[19] K. Ito and V. Vitek, Philos. Mag. A **81**, 1387 (2001).

[20] T. Suzuki, S. Takeuchi, and H. Yoshinaga, *Dislocation Dynamics and Plasticity* (Springer-Verlag, Berlin, 1991).
[21] D. Caillard and J. L. Martin, *Thermally Activated Mechanisms in Crystal Plasticity* (Pergamon Press, Amsterdam, 2003).
[22] J. E. Dorn and S. Rajnak, Trans. AIME **230**, 1052 (1964).
[23] R. Gröger and V. Vitek, Acta Mater. **56**, 5426 (2008).
[24] R. Gröger and V. Vitek, Acta Mater. **61**, 6362 (2013).
[25] C. R. Weinberger, C. C. Bataille, T. E. Buchheit, and E. A. Holm, Int. J. Plast. **37**, 16 (2012).
[26] H. Lim, C. R. Weinberger, C. C. Battaile, and T. E. Buchheit, Modell. Simul. Mater. Sci. Eng. **21**, 045015 (2013).
[27] K. Srivastava, R. Gröger, D. Weygand, and P. Gumbsch, Int. J. Plast. **47**, 126 (2013).
[28] G. Po, Y. Cui, D. Rivera, D. Cereceda, T. D. Swinburne, J. Marian, and N. Ghoniem, Acta Mater. **119**, 123 (2016).
[29] R. Gröger, A. G. Bailey, and V. Vitek, Acta Mater. **56**, 5401 (2008).
[30] S. Xia and A. El-Azab, Modell. Simul. Mater. Sci. Eng. **23**, 055009 (2015).
[31] A. N. Stroh, J. Math. Phys. **41**, 77 (1962).
[32] J. P. Hirth and J. Lothe, *Theory of Dislocations*, 2nd ed. (Wiley, New York, 1982).
[33] R. J. Arsenault, in *Plastic Deformation of Materials*, edited by R. J. Arsenault (Academic Press, New York, 1975), Vol. 6, pp. 1–99.
[34] R. Gröger and V. Vitek, Int. J. Mater. Res. **100**, 315 (2009).
[35] Q. Qin and J. L. Bassani, J. Mech. Phys. Solids **40**, 813 (1992).
[36] R. Gröger, V. Racherla, J. L. Bassani, and V. Vitek, Acta Mater. **56**, 5412 (2008).
[37] R. Zwanzig, *Nonequilibrium Statistical Mechanics* (Oxford University Press, Oxford, 2001).
[38] A. Arsenlis and D. M. Parks, J. Mech. Phys. Solids **50**, 1979 (2002).
[39] D. Hull and D. J. Bacon, *Introduction to Dislocations*, 3rd ed. (Pergamon Press, New York, 1984).
[40] H. L. Prekel, A. Lawley, and H. Conrad, Acta Metall. **16**, 337 (1968).
[41] A. Seeger and W. Wasserbäch, Phys. Status Solidi A **189**, 27 (2002).
[42] K. Kitajima, Y. Aono, and E. Kuramoto, Scr. Metall. **15**, 919 (1981).
[43] Y. Aono, E. Kuramoto, D. Brunner, and J. Diehl, *Strength of Metals and Alloys (ICSMA8): Proceedings of the 8th International Conference* (Pergamon Press, New York, 1989), pp. 271–276.
[44] P. J. Jeffcoat and B. L. Mordike, Z. Metallkd. **70**, 38 (1979).
[45] P. J. Jeffcoat, B. L. Mordike, and K. D. Rogausch, Philos. Mag. **34**, 583 (1976).
[46] C. Marichal, H. Van Swygenhoven, S. Van Petegem, and C. Borca, Sci. Rep. **3**, 2547 (2013).
[47] C. Marichal, K. Srivastava, D. Weygand, S. Van Petegem, D. Grolimund, P. Gumbsch, and H. Van Swygenhoven, Phys. Rev. Lett. **113**, 025501 (2014).
[48] C. J. Bolton and G. Taylor, Philos. Mag. **26**, 1359 (1972).
[49] M. H. A. Nawaz and B. L. Mordike, Z. Metallkd. **66**, 644 (1975).
[50] G. Taylor, R. Bajaj, and O. N. Carlson, Philos. Mag. **28**, 1035 (1973).